White luminescence from Si^+ and C^+ ion-implanted SiO_2 films

A. Pérez-Rodríguez,[a] O. González-Varona, B. Garrido, P. Pellegrino, and J. R. Morante
EME, Departament d'Electrònica, Universitat de Barcelona, Martí i Franquès 1, 08028 Barcelona, Spain

C. Bonafos, M. Carrada, and A. Claverie
CEMES-CNRS, 29 rue J. Marvig, 31055 Toulouse, France

(Received 3 January 2003; accepted 4 April 2003)

The microstructural and optical analysis of SiO_2 layers emitting white luminescence is reported. These structures have been synthesized by sequential Si^+ and C^+ ion implantation and high-temperature annealing. Their white emission results from the presence of up to three bands in the photoluminescence (PL) spectra, covering the whole visible spectral range. The microstructural characterization reveals the presence of a complex multilayer structure: Si nanocrystals are only observed outside the main C-implanted peak region, with a lower density closer to the surface, being also smaller in size. This lack of uniformity in their density has been related to the inhibiting role of C in their growth dynamics. These nanocrystals are responsible for the band appearing in the red region of the PL spectrum. The analysis of the thermal evolution of the red PL band and its behavior after hydrogenation shows that carbon implantation also prevents the formation of well passivated Si/SiO_2 interfaces. On the other hand, the PL bands appearing at higher energies show the existence of two different characteristics as a function of the implanted dose. For excess atomic concentrations below or equal to 10%, the spectra show a PL band in the blue region. At higher doses, two bands dominate the green–blue spectral region. The evolution of these bands with the implanted dose and annealing time suggests that they are related to the formation of carbon-rich precipitates in the implanted region. Moreover, PL versus depth measurements provide a direct correlation of the green band with the carbon-implanted profile. These PL bands have been assigned to two distinct amorphous phases, with a composition close to elemental graphitic carbon or stoichiometric SiC. © *2003 American Institute of Physics.* [DOI: 10.1063/1.1578172]

I. INTRODUCTION

Semiconductor nanocrystals and related nanostructures have been extensively studied in the last years due to their interesting optical and optoelectronic properties. These properties differ significantly from those of the bulk material, due to the presence of quantum confinement of excitons in the nanoparticles.[1–3] This leads to a widening of the band gap, as well as an enhancement of the efficiency of radiative recombination processes. Strong room-temperature photo- and electroluminescent signals have been observed from Si-related structures, such as porous Si or Si nanocrystals embedded in SiO_2.[4,5] These results have opened extremely interesting perspectives for the development of a Si-based optoelectronic technology.

For the development of light-emitter devices in the visible region, one of the most interesting approaches is the synthesis of nanocrystals embedded in a SiO_2 film. SiO_2 is a well-known material from the standard Si technology, transparent in the infrared (IR) and visible spectral range, and it forms highly stable and well-passivated interfaces with silicon.

The ion beam synthesis of Si nanocrystals in SiO_2 is a two-step process which involves: (i) High dose Si ion implantation in a previously thermal oxidized Si wafer and (ii) high-temperature annealing. Thermal treatment of the Si-rich SiO_2 films at temperatures above 900 °C leads to phase separation into nanocrystalline Si and SiO_2 and annealing of the implantation-induced damage.[6,7] The complete recovering of the high structural quality of the initial SiO_2 layer and the very stable and defect-free interface with the nanoparticles are the key features which explain the high photoluminescence (PL) efficiency of these structures.[7,8] The same processes have also been recently used for the fabrication of electroluminescent devices.[9]

The ion beam synthesis of Si nanocrystals in SiO_2 has been the object of extensive investigation including the interpretation of the growth kinetics. This has been modeled by means of predictive simulations of the Ostwald ripening of spherical particles.[7,8,10–12] Besides, the dependence of the average size of the nanocrystals on the processing parameters (ion dose, annealing temperature and time) has also been described in detail. In all of these cases, the emission is located in the red-IR spectral region (1.4–1.8 eV) even for the smallest sizes.[13] Then, luminescent systems at higher energies require alternative nanoparticles with a different chemical composition.

In this framework, the ion beam synthesis of luminescent structures by sequential Si^+ and C^+ ion implantation into the SiO_2 matrix has been proposed.[14–16] In SiO_2 films implanted only with C^+ ions, it has been early evidenced

[a]Author to whom correspondence should be addressed; electronic mail: perez-ro@el.ub.es

that a severe drawback consists in the strong outdiffusion of the implanted C during the thermal process. This is caused by the formation of highly mobile CO species. Accordingly, these phenomena could be prevented by annealing under high-vacuum conditions. However, the most interesting approach to stabilize the implanted C profile is the previous existence of a high Si supersaturation, which enhances the interaction of both C and O atoms with the Si ones, and prevents the formation of C—O bonds. In this respect, Si-rich SiO_2 layers have been demonstrated to act as efficient barriers for C outdiffusion.[17]

High dose sequential implantation of Si^+ and C^+ ions into the SiO_2 oxides followed by high-temperature annealing results in the synthesis of structures with intense white (to the eye) luminescence. This white emission is resulting from the convolution of up to three luminescence bands located in the red-IR, green, and blue spectral regions. They have been related to the formation of different kinds of nanoparticles, such as Si, SiC, and C graphiticlike ones.[18] In a previous experiment, even some evidence of the presence of 6H–SiC precipitates was observed.[19] However, a further detailed analysis on a wider set of samples has not provided a clear hint of the presence of this specific phase.

Intense room-temperature luminescent bands in the blue spectral region as result of C^+ ion-implantation processes into SiO_2 layers have been reported by several authors.[20–22] There is a general consensus in assigning these bands to the formation of C-related nanoparticles. An additional important feature is their very short lifetime (below one microsecond) compared to the Si nanocrystal-related one, which is of the order of hundreds of milliseconds. Zhao *et al.*[23] have reported decay times in the picosecond range. These data are quite relevant in view of the development of optoelectronic emitters, where the competitive switching characteristics rely on fast decay rates. All this gives a strong interest in achieving a more mature knowledge on the mechanisms related to these visible luminescence bands as well as on the physicochemical nature of the synthesized phases.

In this framework, this work reports the detailed structural and optical characterization of luminescent systems synthesized by high dose sequential Si^+ and C^+ ion implantation. The observed visible PL has been correlated with the implant and annealing conditions and with the microstructure of the processed films. The analysis of the interaction mechanisms between both implanted species in the oxide layers has been carried out by means of a wide range of different techniques, such as transmission electron microscopy (TEM), Raman scattering, secondary ions mass spectroscopy (SIMS), and x-ray photoelectron spectroscopy (XPS).

II. EXPERIMENTAL DETAILS

SiO_2 films, 400 nm thick, were grown on *p*-type Si ⟨100⟩ wafers by wet oxidation at 1100 °C. A two-steps Si^+ implantation was designed by TRIM simulations[24] to obtain a rectangular-shaped Si excess profile at depths between 100 nm and 300 nm in the oxide layer. This was made to enhance C blocking and formation of SiC compounds in the implanted layer. Different doses were selected to obtain an excess atomic content of Si in this region between 1% and 30%. Subsequently, a 60 keV C^+ ion implantation was performed to a nominal dose as to obtain a peak C concentration equal to the Si excess value. The implant energy was selected to obtain the C-implanted distribution centred in the Si-rich buried region. All the implantations were performed at room temperature. Table I summarizes the implantation conditions for all the different wafers.

TABLE I. Implantation parameters for the wafers implanted with Si^+ and C^+ ions.

Si and C excess (at. %)	130 keV Si^+ dose (cm^{-2})	60 keV Si^+ dose (cm^{-2})	60 keV C^+ dose (cm^{-2})
1	1.3×10^{16}	5×10^{15}	1×10^{16}
5	6.5×10^{16}	2.5×10^{16}	5×10^{16}
10	1.3×10^{17}	5×10^{16}	1×10^{17}
20	2.6×10^{17}	1×10^{17}	2×10^{17}
30	4×10^{17}	1.5×10^{17}	3×10^{17}

Additionally, reference wafers were implanted only with Si. In this case, a 150 keV Si^+ ion implantation was performed at room temperature to doses ranging from 10^{16} to 3×10^{17} Si^+/cm^2. The implant parameters were tailored in order to obtain a projected range of about 200 nm and a silicon peak concentration similar to the one in Table I.

The samples were annealed under N_2 atmosphere at 1100 °C in two steps: The initial one was in a rapid thermal processing system (1 min) to ensure the reproducibility of the process, while the second one was performed in a conventional furnace (annealing time up to 16 h). This wide range of annealing times allows one to closely follow the Si precipitate evolution through the whole ripening regime, where the nucleation and pure growth are completed after the first minutes. In addition, some selected samples underwent postannealing treatment in forming gas (95% N_2 + 5% H_2) at 450 °C during 20 min.

PL measurements have been performed using a 60 mW He–Cd laser for ultraviolet excitation ($\lambda = 325$ nm). The luminescent emission was analyzed in backscattering mode by a 0.6 m monochromator and detected with a GaAs photomultiplier. The standard chopper-lock-in technique was used to increase the signal-to-noise ratio.

PL versus depth profiles on selected samples were performed by scanning PL microscopy on the surface of low angle bevelled samples (nominal bevel angle of 8°). Bevelling was made by mechanical polishing, using a commercial SSM Spreading Resistance Probe system. The sample was excited with a He–Cd laser and the light was recollected with an Olympus metallographic microscope provided with a reflection objective (numerical aperture of 0.4), which allows one to achieve a lateral resolution of about 1 μm.

The detection and analysis of C-related phases was performed by Raman scattering and XPS measurements. Raman scattering measurements were made in backscattering configuration with a Jobin–Yvon T64000 spectrometer coupled with an Olympus metallographic microscope using the blue line of an Ar^+ laser ($\lambda = 488$ nm) as excitation light. The laser power density in the sample was kept below 800 kW/cm^2 to avoid thermal effects. XPS spectra were mea-

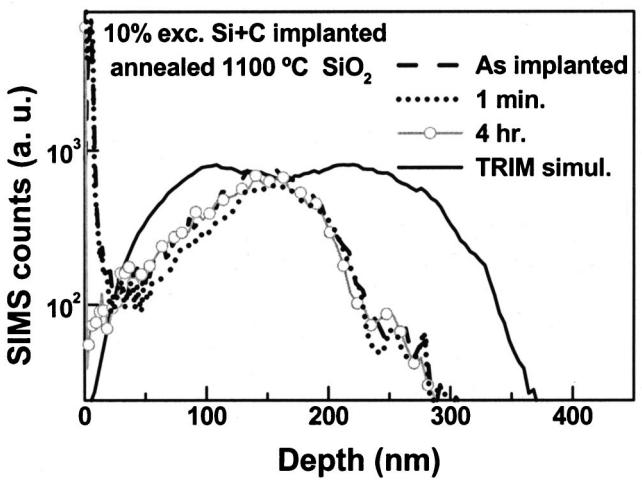

FIG. 1. SIMS profile of the C concentration in the 10 at. % exc. Si+C coimplanted wafer, before and after annealing at 1100 °C. The Si-implanted profile has been added, as simulated by TRIM.

sured with a Perkin–Elmer PHI-5500 instrument using Al $K\alpha$ radiation. XPS versus depth profiles were obtained by measuring the spectra after sputtering the samples to different thicknesses with an Ar^+ ion beam at 4 keV.

For the microstructural characterization of the wafers, the TEM technique has also been used. Cross-sectional (XS) TEM was used to identify the different crystalline phases present in the implanted oxides, as well as to characterize the size distribution of the nanocrystal population in the different regions of the samples and their evolution with the dose and annealing time. High-resolution electron microscopy and bright-field observations were performed by using a Philips CM30 microscope at XS samples. Some of these samples have also been studied under dark-field conditions by using a JEOL 200CX microscope for size-distribution measurements only.

Finally, the distribution to the C-implanted atoms has been also assessed by SIMS measurements using an Atomika A-DIDA 3000-30 spectrometer with an O^+ primary ion source at 6 keV and an electron gun for charge neutralization.

III. RESULTS AND DISCUSSION

A. Characterization of the C-implanted profile and C-related phases

Figure 1 shows the C depth profiles measured by SIMS in samples implanted with 10% excess, both as implanted and annealed for different durations. The Si-implanted profile, as simulated by TRIM, is also included. Figure 1 also shows the presence of a narrow surface C peak in the samples as implanted and annealed for 1 min. This surface peak vanishes when annealing is performed for longer times (more than 10 min). It is apparent that the C profile is kept well centered in the Si-rich region, even after annealing for 16 h. This clearly demonstrates the ability of the initial Si^+ implant to inhibit the formation of C—O phases by stabilizing the C profile.

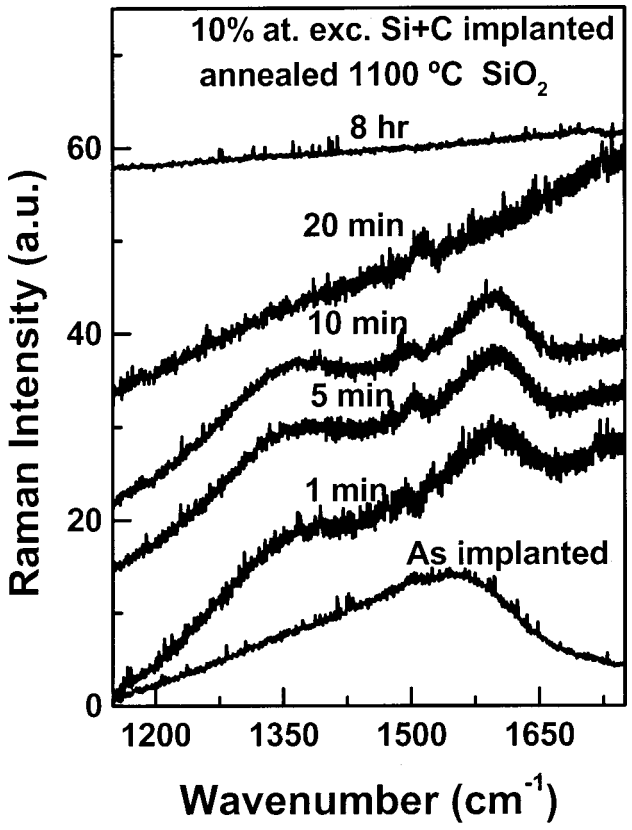

FIG. 2. Raman spectra of the 10 at. % exc. Si+C coimplanted and annealed wafer. For more clarity, the spectra have been vertically shifted. The small feature appearing in some spectra at about 1500 cm^{-1} is an artifact from the detector system.

The Raman spectra measured in the 1200–1700 cm^{-1} spectral region at the same set of samples after thermal treatment at 1100 °C for different durations are displayed in Fig. 2. The as-implanted sample shows a broadband contribution, centered at about 1500–1600 cm^{-1}. This is similar to that previously measured in amorphous C and SiC films.[25,26] This indicates the existence in the as-implanted samples of C—C related vibrational modes from an amorphous phase. After annealing, this band evolves toward two distinct contributions: The E_{2g} graphite vibrational mode at 1360 cm^{-1} and a zone-edge mode at 1590 cm^{-1}. This last mode is active as a consequence of the disorder-induced relaxation of the k-conservation rule.[27] Therefore, thermal treatment leads to the formation of sp^2 coordinated C—C bonds in an amorphous or highly disordered phase. For annealing times longer than 10 min, these bands disappear in accordance with the vanishing of the surface C layer after oxidation.

The Raman spectra (not shown) for samples implanted at different doses and annealed during 4 h show an interesting feature: After such a long thermal treatment, only the sample implanted with 20% Si and C excess shows a contribution from sp^2 coordinated vibrational modes, implying the presence of a high amount of carbon in graphitic phases in the implanted region.

A systematic XPS analysis has been carried out on the processed structures. A typical concentration profile in an

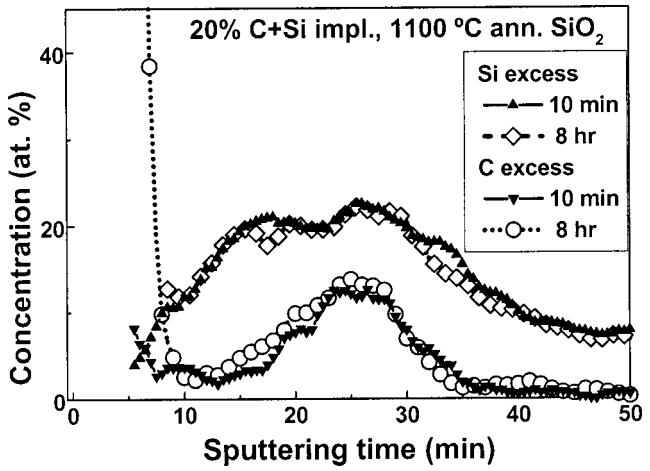

FIG. 3. Concentration vs depth profiles for the implanted species as obtained by XPS measurements on the 10 at. % exc. Si+C coimplanted and annealed sample.

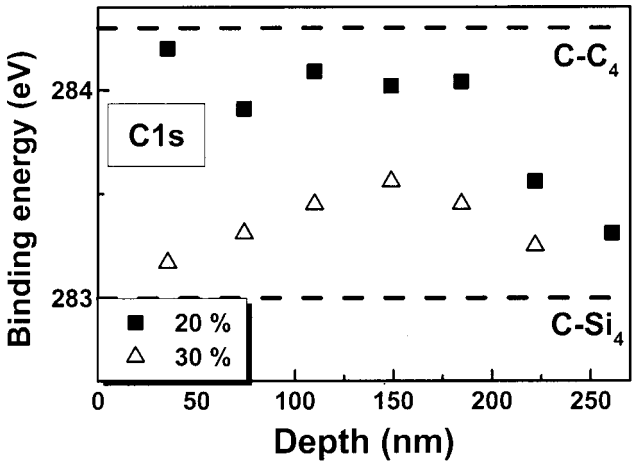

FIG. 4. Energy position vs depth profile for the C 1*s* peak as obtained by XPS measurements on the 20 and 30 at. % exc. Si+C coimplanted and annealed samples.

annealed sample is shown in Fig. 3. The C atomic content at the surface is up to 40% in this case, and it extends up to about 10–20 nm in depth. The corresponding XPS band is centered at 284.3 eV, and is characteristic of carbon bonded to four C atoms (C—C_4). This gives additional support to the assignment of the graphite signal from the Raman spectra to this C-rich surface region. The origin of the high carbon content in this surface layer has to be related to a contamination of the beam during the implantation. The thermal stability of the implanted profile is well demonstrated also by the XPS profiles of annealed samples.

We checked that the whole C-implanted profile is proportional to the implanted dose, and it does not show any sign of broadening when increasing the implanted dose or annealing time. The C signal in the implanted region has a maximum content at a depth of about 150 nm. The position of the C XPS peak always ranges between those positions characteristic of graphite (284.3 eV, C—C_4) and SiC (282.8 eV, C—Si_4). In principle, this variation could be related to the presence of C-rich SiC complexes in the implanted region, or to the coexistence of two different C-related phases, as graphite and Si-rich SiC.

In Fig. 4, the energy position of the C 1*s* band versus depth is represented for the samples implanted to the highest doses (corresponding to 20% and 30% of implanted excess atoms). In the other cases, their intensity is too low to allow a reliable analysis. As reference, we have also indicated the positions corresponding to both C—C_4 and C—Si_4 bonding configurations. The relative position of the experimental band in relation to these references provides an indication of the relative amount of C in the respective phases. It is apparent that the predominance of the graphite phase in the sample implanted with 20% excess atoms, while for the sample with 30% excess atoms there is a significant shift toward the SiC phase. A fitting of the spectra with two Gaussian contributions centered at the reference positions allows one to estimate the relative weight of each phase. For the sample implanted with 20% excess atoms, about 75% of implanted C is in the graphite phase and only about 25% of the atoms are bonded to Si in a SiC phase. On the other hand, these fractions are of 40% and 60%, respectively, in the other sample (30% excess atoms). These data agree well with the Raman measurements. As previously indicated, only for the samples implanted with 20% excess atoms, there is a remaining detectable contribution in the Raman spectra from graphite vibrational modes after a long annealing time.

In the XPS Si 2*p* spectrum the Si—C (at 100.2 eV) and Si—Si (at 99.6 eV) components have not been resolved, due to their small energy separation. However, in the regions outside the C-implanted peak, the Si-related XPS band presents a well pronounced shoulder on the low-energy side, corresponding to the signal characteristic of Si—Si_4 bonding configuration at 99.6 eV. This implies the existence of pure Si aggregates in these portions of the implanted layer.

B. Detection and characterization of Si nanocrystallites

The XS TEM analysis of the implanted and annealed samples has revealed the existence of a complex multilayer structure, as can be seen in Fig. 5. This corresponds to the sample implanted with a 30% excess of Si and C and annealed during 16 h. Figure 5 shows the presence of a buried layer with a darker contrast where no crystalline precipitates are detected (labeled as region 2 in the TEM image). Moreover, in the regions next to the buried layer (regions 1 and 3, respectively), a population of small nanocrystals has been observed. The analysis of the nanodiffraction patterns from these regions has allowed us to identify them as Si nanocrystals. The inset in Fig. 5 shows a high-resolution TEM image of one of these nanocrystals from region 1. Finally, region 4 corresponds to the remaining SiO_2 layer, without precipitates.

In Fig. 6, the Si nanocrystal mean diameter and standard deviation from both regions 1 and 3 are represented as a function of the excess of implanted atoms. These data have been measured for the samples implanted with 10%, 20%, and 30% excess and annealed for 16 h. Data obtained from Si-implanted reference samples have been added. All of

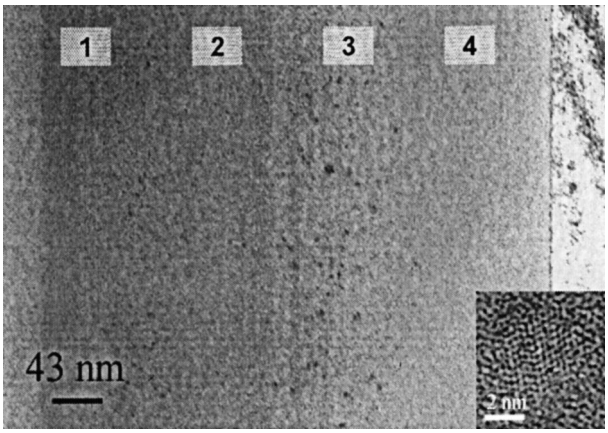

FIG. 5. XS TEM image of the 30 at. % exc. Si+C implanted and annealed (16 h) sample. The image shows the presence of a buried layer with darker contrast and free of crystalline precipitates (region 2). Comparison with the implanted profiles indicates that this region corresponds to the maximum of the C-implanted profile. Si nanocrystals are observed in regions 1 and 3, which are located above and below this buried layer. Finally, region 4 corresponds to the remaining SiO_2 layer without precipitates. The inset shows a high-resolution image of a Si nanocrystal from the region 1, above the buried C layer.

these values have been obtained from the corresponding size histograms, which were measured by detailed TEM observations under dark-field imaging conditions at a significant number of precipitates (higher than 50). For the samples implanted to lower doses, the number of precipitates observed was not high enough to obtain reliable statistics. The measurements were performed using dark-field conditions for the imaging of Si nanocrystals in SiO_2, as described in Ref. 14.

A comparison of Fig. 5 with the Si^+- and C^+-implanted profiles reveals the strong dependence of the microstructure in each region with the relative C to Si ratio: Region 2 corresponds to the maximum of the C-implanted profile, where both Si and C excess contents are similar. The high C content in this region strongly inhibits the precipitation of Si in the nanocrystalline form. Most of the Si excess atoms are probably trapped in SiC-related complexes which are not resolved in the TEM image but detected by XPS. The formation of the nanocrystals is only possible in regions 1 and 3, where the concentration of C atoms is well below the Si-implanted one. Furthermore, a noticeable decrease is apparent in the average size of the Si nanocrystals of region 1 in respect to those observed in region 3 (i.e., 1.1 nm against 1.4 nm for 10% Si excess). The implanted species profile versus depth in Figs. 1 and 3 reveals that the ratio between C- and Si-implanted atoms is higher in region 1 than in region 3. Moreover, the average size of the Si nanocrystals is always larger for the reference samples not containing carbon. Thus, the different density and size distribution in regions 1 and 3 is likely due to a preferential bonding of Si with C atoms.

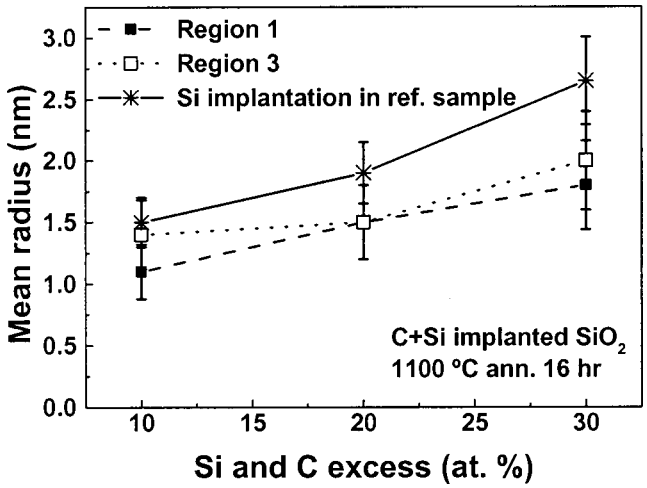

FIG. 6. Mean radius of the Si nanocrystals in the region 1 and 3 as a function of the implanted Si and C excess concentration, as obtained by statistical evaluation of TEM measurements. For comparison, data have been added from reference samples implanted only with Si.

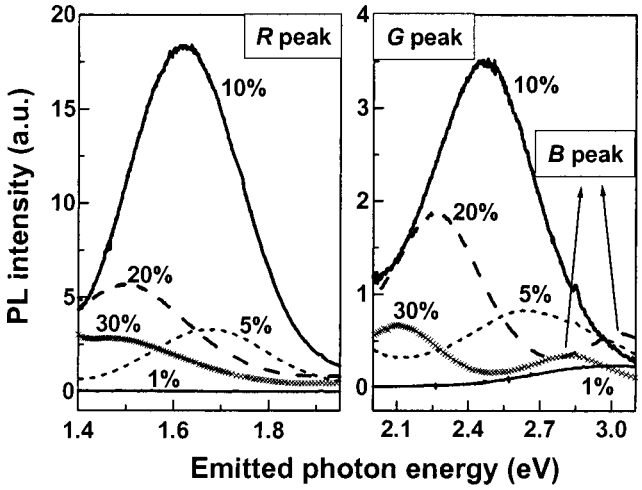

FIG. 7. PL spectra from samples implanted with different excess concentrations of Si and C. The samples have been annealed at 1100 °C for 2 h.

C. Optical analysis: Photoluminescence behavior

As already mentioned, the oxides coimplanted with Si^+ and C^+ ions show, after annealing, an intense luminescence signal visible to the naked eye. For Si- and C-implanted contents of 10% or higher, this luminescence appears as an intense white emission. This results from the simultaneous emission of up to three bands covering the whole visible spectral range from the red to the blue region.

Fig. 7 shows the PL spectra measured from the samples implanted with the different excess concentrations after annealing for 2 h. The spectra always present a band in the red-IR region, as plotted in Fig. 7 (left-hand side). In the following, it will be labeled as the *R* band. The samples implanted to doses leading to excess Si and C contents up to 10% show a additional band in the blue–green spectral region, labeled as the *G* band (see Fig. 7, right-hand side). Finally, the samples implanted to higher doses show a third luminescence band in the blue wavelength range, labeled as the *B* band.

The peak energy of these three bands as a function of the atomic excess concentration is plotted in Fig. 8, together with data from the reference samples. The spectral position of the *R* band shows the same dependence on the implanted dose as the red-IR emission characteristic of Si nanocrystals.

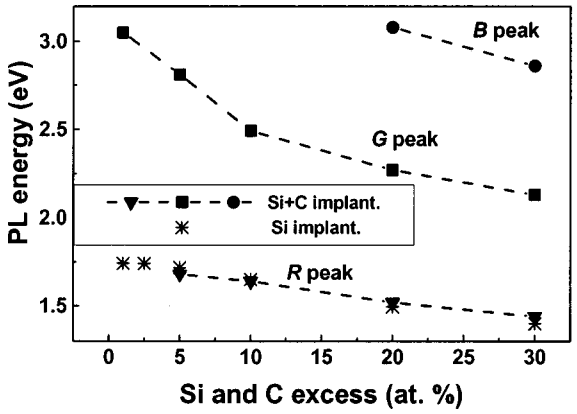

FIG. 8. PL energy position of the *R*, *G*, and *B* peaks as a function of the implanted Si and C atomic excess concentration.

This allows the assignment of this band to these nanoprecipitates. As shown in a previous work,[8] for doses leading to Si excess content below 10%, the average size of the nanocrystals does not depend on the implanted dose, and the corresponding PL emission is centered at about 1.7–1.8 eV. For higher doses, interaction effects between the Si nanocrystals lead to an increase in the average size (as shown in Fig. 6), and it determines a redshift of the PL band, according to the quantum confinement effect. The other PL bands show a similar shift as the implanted dose increases. This is apparent in particular for the *G* band, which evolves from the blue region for a carbon content below 10% to the green one for the other cases. In this case, such a large redshift has to be attributed to a variation in the composition and/or atomic configuration of the carbon aggregates, rather than to quantum confinement effects characterized by the size increase of the particles with the implanted dose.

The kinetic evolution of the intensity of the *R* and *G* bands is plotted in Fig. 9. The *R* band shows a strong increase with the annealing time. However, in almost all of the samples, a saturation is not reached even after the longer annealing time of 16 h. As described in previous studies, the evolution of the PL intensity with the annealing time of Si nanocrystals ion beam synthesized in SiO_2 is characterized by the existence of two distinct regimes; (i) an initial fast increase (transient stage) that bends over after 3–4 h of annealing and (ii) a saturation regime for longer annealing times up to 16 h. Once the nanocrystal population has reached the asymptotic Ostwald ripening stage (after about a few minutes by annealing at 1100 °C), any further increase in PL efficiency is mainly related to the progressive passivation of interfacial nonradiative defects, such as P_b centers. This has been established by observing an inverse correlation between the PL intensity and the density of P_b defects measured by the electron spin resonance technique for annealing times longer than 20 min.[7,8]

The observation of a different thermal evolution of the *R* band (no saturation in intensity) under the actual experimental conditions suggests that the presence of C atoms slows down the kinetics of formation of the Si nanocrystals and/or their interface passivation. To further investigate this issue, additional thermal treatments have been performed in forming gas ($N_2=95\%, H_2=5\%$) ambient. Previous studies on Si-implanted SiO_2 have demonstrated that hydrogenation at moderate temperatures considerably enhances the PL intensity and lifetime of the Si nanocrystal-related band, by passivating P_b interfacial defects.[8]

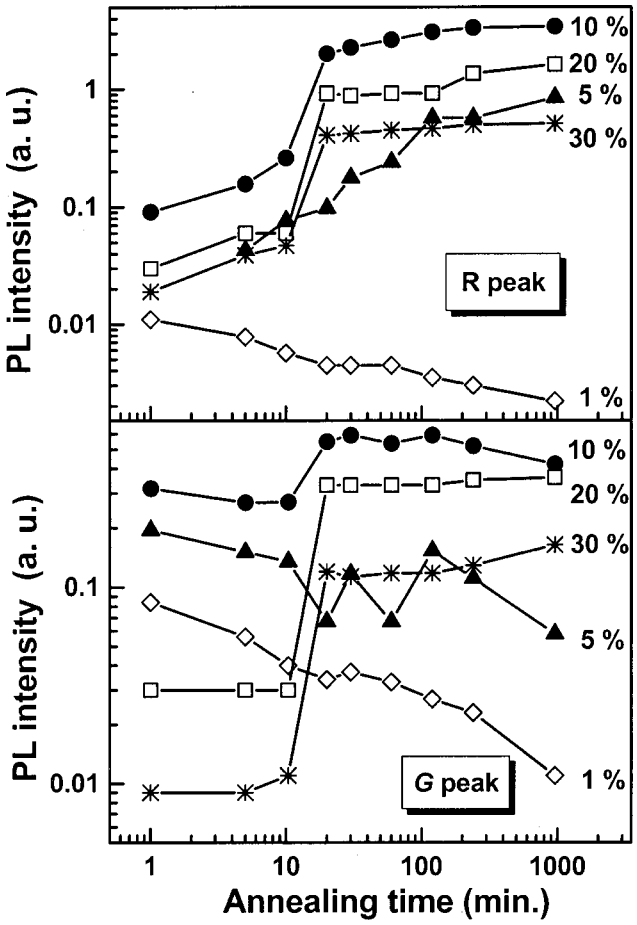

FIG. 9. PL intensity of the *R* and *G* peaks as a function of the annealing time for the different implanted Si and C excess.

The red emission from the sample implanted with 30% excess of Si^+ and C^+ ions and annealed at 1100 °C during 20 min increases by a factor of 5 after forming gas annealing (450 °C, 20 min), while keeping the same spectral shape (not shown). For the higher-energy bands, no significant changes are observable. A similar behavior has also been obtained in the sample implanted with the same dose and annealed during 8 h, leading to the conclusion that even after the longest annealing times a significant density of nonradiative defects is still present at the Si/SiO_2 interface. This observation suggests an active role of the implanted C atoms in inhibiting the formation of well-passivated Si/SiO_2 interfaces. An alternative explanation which, in principle, cannot be ruled out, considers the damage accumulation in the implanted layer as a consequence of the extremely high doses used in the present experiment. A high density of point defects in such structures could account for the reduction in optical efficiency of the Si nanostructures, either after standard high-temperature annealing in inert atmosphere or after hydrogenation.

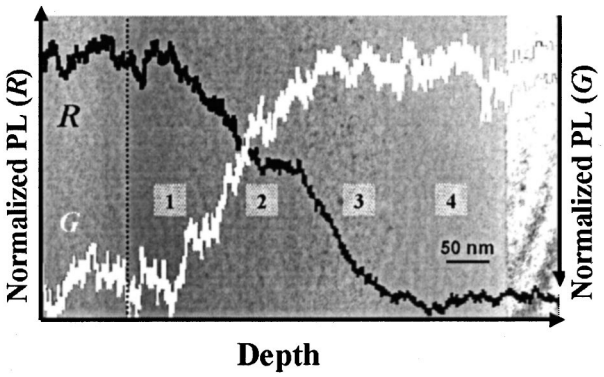

FIG. 10. Normalized PL intensity of the *R* and *G* peaks vs depth profiles from the sample implanted with 20% excess atoms and annealed for 10 h. The labelling indicates the regions with different C content.

For the *G* band, the data on the PL intensity versus annealing time plotted in Fig. 9 show the existence of a more complex behavior. In fact, two different trends are observed depending on the implanted dose: (i) For doses leading to implanted excess atom concentrations below 10%, the *G* band slowly vanishes for increasing annealing duration, while (ii) for doses exceeding this value, the intensity of the band increases and shows a fast transient stage toward saturation for annealing times between 10 and 20 min. The 10% excess case shows an intermediate behavior between both cases.

For the higher implanted doses, the *G* band shifts from the blue to the green spectral region, while the PL intensity presents an evolution characteristic of the growth kinetics of particles in the SiO_2 matrix. As a function of the implanted dose, the PL intensity at the saturation regime shows a nonmonothonic behavior, with a maximum emission for a 10%–20% excess. The intensity of the *B* band, only detected for the higher implanted doses (not shown in Fig. 9), presents a similar behavior.

Figure 10 shows the results of the indepth resolved scanning PL measurements. The intensity of both *R* and *G* bands (versus depth) has been measured at different points from the low angle bevelled surface of the sample implanted with 20% excess atoms and annealed for 10 h. The XS TEM image of the sample has been added in the background and, for more clarity, the *y* axis for the normalized intensity of the *G* band has been inverted. The evolution of the *B* band is hindered by a parasitic component in the experimental setup, which did not allow its indepth resolved analysis. Figure 10 shows that the intensity of the *R* band decreases when the laser spot passes through the shallower (region 1) and deeper (region 3) layers containing Si nanocrystals, while it remains constant through the region 2 (without Si nanocrystals). Such direct experimental evidence provides a definitive identification of this band as related to the Si nanocrystals. On the other hand, the intensity of the *G* band closely follows the C-implanted profile. It decreases when scanning region 1 and mostly region 2, while the signal becomes negligible once the laser spot has reached region 3. Such a direct correlation of the *G* band with the C-implanted profile ensures that the observed optical features in the green spectral range are indeed related to carbon clusters mainly located in region 2.

The presence of two well resolved bands (*G* and *B*) in the case of samples implanted to the highest doses can be correlated with the existence of two distinct phases involving the C-implanted atoms, according to the interpretation of the XPS experiments: Graphitic carbon and SiC. The detailed TEM observation of region 2 (including high-resolution imaging and electron nanodiffraction) has not shown any signal from a crystalline phase, implying the probable amorphous nature of these precipitates. We have to notice that the detailed composition of these precipitates is not well established. Although the XPS data are explained in terms of both graphitic elemental carbon and stoichiometric SiC, this could alternatively be determined by Si_xC_y (or even $Si_xC_yO_z$) domains with different composition, still close to elemental carbon and stoichiometric SiC. This has been confirmed by electron energy loss spectroscopy measurements on the same set of samples, which detected the presence of $Si_xC_yO_z$ complexes (data not yet published).

The assignment of the *G* and *B* bands from the samples implanted at the higher doses to the C-rich and SiC-related precipitates is in accordance with the structural analysis. The samples with the highest relative contribution of the *G* band in the PL spectrum are those implanted with 20% excess atoms. These are also the samples with a highest relative amount of carbon bonded in the graphitic phase. The same set is also the only one that shows a remaining graphitic contribution in the Raman spectra after a long annealing time, as previously pointed out. Increasing the Si^+- and C^+-implanted dose leads to an enhancement of the SiC-related phase, and this is also accompanied by an increase in the relative intensity of the *B* band in respect to the *G* one.

The proposed interpretation for the *G* and *B* bands is also supported by the data reported in literature. Hayashi *et al.*[28] observed a broad luminescence band centered at about 2.2 eV from C-rich SiO_2 films prepared by rf cosputtering, and the position of this band shifts toward higher energies when the C content decreases. This behavior, together with the Raman and optical absorption data, has led to the interpretation that this band is related to carbon clusters in the oxide. A yellow–green luminescence band (2.0–2.2 eV) was also observed in C ion-implanted SiO_2 layers. In this case, the intensity of the PL band was well correlated with the contribution of carbon-related vibrational modes in the Raman spectra.[14] A luminescence band at higher energies, in the range from 2.5 eV to 2.95 eV, has also been reported from carbon graphite microcrystals embedded in SiO_2 layers synthesized either by ion implantation[22,23] or by sputtering deposition of C-rich oxides[29] followed by thermal annealing. It is worth remarking upon the strong dependence of the PL energy on the conditions of fabrication of the samples, which determines the carbon cluster structure and size.

Blue luminescent bands in the region 2.4 eV–2.8 eV are also characteristic of SiC-related crystalline nanostructures, as porous SiC.[30–35] Besides, some authors have analyzed the PL emission from Si^+ and C^+ ion-implanted SiO_2.[20,21] Rebohle *et al.*[21] have reported the appearance of two bands close to the *G* and *B* ones, at about 2.1 eV and 2.9 eV, in a Si^+ and C^+ sequential implantation process with excess

atomic concentration in the range of 5% to 10%.[21] The absence of the *R* band related to the Si nanocrystals was due to the fact that both Si and C implant conditions were chosen to obtain similar overlapping excess Si and C profiles. TEM observations in these samples corroborated the absence of nanocrystals in the implanted layer. They attributed the high-energy band (2.7–2.8 eV) to the formation of amorphous clusters of $Si_yC_{1-y}O_x$ complexes. Quite interestingly, they point out that a different origin of the blue emission, for instance from implantation-induced point defects, can be ruled out. This is a particularly important point to discuss in the present interpretation of the results for the low-implanted doses (1% and 5% excess), where, apparently, the *G* band shows two anomalies: The PL peak appears at very high energies (2.8–3.0 eV) and it shows a lower thermal stability. The formation of oxygen-vacancy-related defects in SiO_2 has been previously claimed to interpret the strong blue luminescent signal from Si^+, Ge^+, and Sn^+ ion-implanted SiO_2 specimens.[36,37] These layers show a strong PL signal peaked at energies between 2.7 eV and 3.2 eV, together with an UV emission around 4.3 eV. The intensity of these bands strongly depends on the implanted dose and ion mass (ruling the defect production negligible in the case of carbon), and on the annealing temperature (defect thermal stability). In the case of silicon implantation, the oxygen-vacancy centers are completely annealed out at temperatures above 900–1000 °C and, in fact, no sign of their PL emission has been found in our reference samples.

Moreover, we found out that the lifetime decays of the *B* and *G* bands are in the nanosecond range for the whole set of annealed samples (not shown). This agrees with the available reports on time-resolved measurements. Intense blue PL bands have been reported from thermal SiO_2 films coimplanted with Si^+ and C^+ ions by Zhao *et al.*,[20] related to the formation of SiC and/or Si, C, and O related complexes. They reported lifetime constants ranging from 50 to 800 ps. Lifetime decays from 100 ps up to few ns have also been measured in porous SiC,[30,34] providing an additional indication of the likely relationship of the luminescent *B* band with SiC-related secondary phases in the SiO_2 matrix.

IV. CONCLUSIONS

The detailed microstructural and optical analysis of the Si^+ and C^+ sequentially implanted and annealed SiO_2 layers has allowed us to characterize the different bands arising in the PL spectra, which are responsible for the intense white emission observed at the higher implanted doses (for atomic excess concentrations higher than 10%). These bands have been assigned to the emission from Si nanocrystals, and C-related amorphous nanoparticles with a composition close to graphitic carbon and SiC, respectively. At lower implanted doses, the PL spectra only show one band, in addition to the well-known red one related to the Si nanocrystals. While still being related to carbon-containing clusters, it shows a lower thermal stability. Carbon implantation has also been observed to strongly inhibit the formation of Si nanocrystals in the region of the C-implanted profile, affecting also the growth kinetics of the Si nanocrystals and the passivation of the Si/SiO_2 interfaces. As a result, a proper choice of the implantation and annealing conditions allows one to tune the color and wavelength of the emission, by tailoring the various contributions in the PL spectra.

ACKNOWLEDGMENTS

This work has been partially funded by the project ref. PICS 2001-6 under the ''Generalitat de Catalunya''-CNRS International Program for Scientific Cooperation (PICS).

[1] L. T. Canham, Appl. Phys. Lett. **57**, 1046 (1990).
[2] L. Brus, J. Phys. Chem. **90**, 2555 (1986).
[3] V. Lehmann and U. Gosele, Appl. Phys. Lett. **58**, 856 (1991).
[4] J. C. Vial, A. Bsiesy, F. Gaspard, R. Herino, M. Ligeon, F. Muller, R. Romestain, and R. M. Macfarlane, Phys. Rev. B **45**, 14171 (1992).
[5] T. Shimitzu-Iwayama, S. Nakao, and K. Saitoh, Appl. Phys. Lett. **65**, 1814 (1994).
[6] M. López, B. Garrido, C. Bonafos, A. Pérez-Rodríguez, J. R. Morante, and A. Claverie, Nucl. Instrum. Methods Phys. Res. B **178**, 89 (2001).
[7] B. Garrido, M. López, C. García, A. Pérez-Rodríguez, J. R. Morante, C. Bonafos, M. Carrada, and A. Claverie, J. Appl. Phys. **91**, 798 (2002).
[8] M. López, B. Garrido, C. García, P. Pellegrino, A. Pérez-Rodríguez, J. R. Morante, C. Bonafos, M. Carrada, and A. Claverie, Appl. Phys. Lett. **80**, 1637 (2002).
[9] J. De La Torre, A. Souifi, A. Poncet, C. Busseret, M. Lemiti, G. Bremond, O. González, B. Garrido, J. R. Morante, and C. Bonafos, Phys. Rev. E **16**, 326 (2003).
[10] C. Bonafos, B. Garrido, M. López, A. Pérez-Rodríguez, J. R. Morante, Y. Kihn, B. Ben-Assayag, and A. Claverie, Appl. Phys. Lett. **76**, 3962 (2000).
[11] M. López, B. Garrido, C. Bonafos, A. Pérez-Rodríguez, and J. R. Morante, Solid-State Electron. **45**, 1495 (2001).
[12] C. Bonafos, B. Colombeau, A. Altibelli, M. Carrada, G. Ben Assayag, B. Garrido, M. López, A. Pérez-Rodríguez, J. R. Morante, and A. Claverie, Nucl. Instrum. Methods Phys. Res. B **178**, 17 (2001).
[13] M. V. Wolkin, J. Jorne, P. M. Fauchet, G. Allan, and C. Delerue, Phys. Rev. Lett. **82**, 197 (1999).
[14] B. Garrido, M. López, S. Ferré, A. Romano-Rodríguez, A. Pérez-Rodríguez, P. Ruterana, and J. R. Morante, Nucl. Instrum. Methods Phys. Res. B **120**, 101 (1996).
[15] M. López, B. Garrido, C. Bonafos, O. González-Varona, A. Pérez-Rodríguez, R. Rodríguez, P. Ruterana, and J. R. Morante, Mater. Res. Soc. Symp. Proc. **486**, 237 (1998).
[16] B. Garrido, C. Bonafos, M. López, A. Cuadras, A. Pérez-Rodríguez, K. Pressel, and J. R. Morante, Defect Diffus. Forum **160**, 1 (1998).
[17] A. Pérez-Rodríguez, B. Garrido, C. Bonafos, M. López, O. González-Varona, and J. R. Morante, J. Mater. Sci. **10**, 185 (1999).
[18] O. Gonzalez-Verona, B. Garrido, A. Pérez-Rodríguez, J. R. Morante, C. Bonafos, M. Carrada, L. F. Sanz, M. A. González, and J. Jiménez, Mater. Sci. Eng., B **91**, 51 (2002).
[19] O. González-Varona, A. Pérez-Rodríguez, B. Garrido, C. Bonafos, M. López, J. R. Morante, J. Montserrat, and A. Rodríguez, Nucl. Instrum. Methods Phys. Res. B **161**, 907 (2000).
[20] J. Zhao, D. S. Mao, Z. X. Lin, B. Y. Jiang, Y. H. Yu, X. H. Liu, H. Z. Wang, and G. Q. Yang, Appl. Phys. Lett. **73**, 1838 (1998).
[21] L. Rebohle, T. Gebel, H. Fröb, H. Reuther, and W. Skorupa, Appl. Surf. Sci. **184**, 156 (2001).
[22] Y. H. Yu, S. P. Wong, and I. H. Wilson, Phys. Status Solidi A **168**, 531 (1998).
[23] J. Zhao, D. S. Mao, Z. X. Lin, B. Y. Jiang, Y. H. Yu, X. H. Liu, and G. Q. Yang, Mater. Lett. **38**, 321 (1999).
[24] J. F. Ziegler, J. Appl. Phys. **85**, 1249 (1999).
[25] R. O. Dillon, J. A. Woollam, and V. Katkanant, Phys. Rev. B **29**, 3482 (1984).
[26] A. Pérez-Rodríguez, Y. Pacaud, L. Calvo-Barrio, C. Serre, W. Skorupa, and J. R. Morante, J. Electron. Mater. **25**, 541 (1996).
[27] D. S. Knight and W. B. White, J. Mater. Res. **4**, 385 (1989).
[28] S. Hayashi, M. Kataoka, and K. Yamamoto, Jpn. J. Appl. Phys., Part 2 **32**, L274 (1993).

[29] Q. Zhang, S. C. Bayliss, and W. Frentrup, Solid State Commun. **99**, 883 (1996).
[30] T. Matsumoto, J. Takahashi, T. Tamaki, T. Fugati, and Y. Kanemitsu, Appl. Phys. Lett. **64**, 226 (1994).
[31] A. O. Konstantinov, A. Henry, C. I. Harris, and E. Janzén, Appl. Phys. Lett. **66**, 2250 (1995).
[32] L. S. Liao, X. M. Bao, Z. F. Yang, and N. B. Min, Appl. Phys. Lett. **66**, 2382 (1995).
[33] W. Shin, W. Seo, O. Takai, and K. Koumoto, J. Electron. Mater. **27**, 304 (1998).
[34] J. P. Conde, V. Chu, M. F. da Silva, A. Kling, Z. Dai, J. C. Soares, S. Arekat, A. Fedorov, M. N. Berberan-Santos, F. Giorgis, and C. F. Pirri, J. Appl. Phys. **85**, 3327 (1999).
[35] T. Ma, J. Xu, J. Du, W. Li, X. Huang, and K. Chen, J. Appl. Phys. **88**, 6408 (2000).
[36] L. Rebohle, J. von Borany, H. Fröb, T. Gebel, M. Helm, and W. Skorupa, Nucl. Instrum. Methods Phys. Res. B **188**, 28 (2002).
[37] L. Rebohle, J. von Borany, H. Fröb, and W. Skorupa, Appl. Phys. B: Lasers Opt. **71**, 131 (2000).